Proceedings of 12th Cambridge Workshop on Cool Stars, Stellar Systems, & The Sun, 2003 University of Colorado.

Time Series Spectropolarimetry of T Tauri Stars[1]

Jeff A. Valenti[2], Christopher M. Johns–Krull[3], Artie P. Hatzes[4]

Abstract. We present 6 nights of spectropolarimetry and simultaneous photometry for the T Tauri stars AA Tau, BP Tau, DF Tau, and DK Tau. We determine net longitudinal magnetic field globally using photospheric absorption lines and in accretion zones using the 5876 Å He I line. We compare changes in magnetic field, broad band photometry, absorption line depths (veiling), line profile morphology, emission line strength, velocity shifts, and line asymmetry. The data constrain magnetic and accretion geometry.

1. Observations

Starting on 1998 November 26, we obtained 6 consecutive nights of simultaneous photometry and R=60 000 spectropolarimetry at McDonald Observatory. We used the Zeeman analyzer constructed by Vogt, Tull, & Kelton (1980) with modifications described in Johns–Krull et al. (1999), except that we used an external achromatic $\frac{1}{2}$ wave plate to switch beam polarization in alternate exposures. Table 1 lists properties (from Johns–Krull & Valenti 2001) of the stars we monitored. Figures 1–28 present temporal variations in measured quantities. Only a subset of these results are discussed in this brief report.

2. Net Longitudinal Magnetic Field, B_z

Figures 1, 8, 15, and 22 show B_z measured from wavelength shifts in spectral lines recorded through right and left circular polarizers (Johns–Krull et al. 1999). Polarization is not detectable in photospheric absorption lines, implying a complex magnetic geometry over most of the stellar surface. He I 5876 Å profiles (Figures 4a, 11a, 18a, and 25a) can be strongly polarized, implying globally organized magnetic field lines connecting the disk with sparse accretion zones on the stellar surface. He I polarization varies smoothly on time scales comparable to stellar rotation, suggesting rotational sweeping of a tilted magnetic

[1]This work supported in part by NASA Origins grant NAG5-8098 to the University of California, Berkeley.

[2]Space Telescope Science Institute

[3]Rice University

[4]Thüringer Landessternwarte Tautenburg

Table 1. Properties of Monitored T Tauri Stars

Star	Spectral Type	P_{rot} (day)	M ($M_\odot$)	R ($R_\odot$)	$\dot{M}$ ($M_\odot$ yr^{-1})	$v \sin i$ (km s^{-1})	i (deg)
BP Tau	K7	7.6	0.49	1.99	0.29×10^{-7}	7 ± 2	~ 50
DF Tau	M2	8.5	0.27	3.37	1.77×10^{-7}	18 ± 4	~ 85
DK Tau	K7	8.4	0.43	2.49	0.40×10^{-7}	12 ± 2	~ 50
AA Tau	M0	8.2	0.53	1.74	0.03×10^{-7}	11 ± 2	~ 70

dipole. The angle between rotational and magnetic axes is $>40^\circ$ for DK Tau, which has a polarization reversal, and $<90^\circ - i$ for the other 3 stars. Polarization measurements are not hampered by changes in accretion rate and line strength.

3. Photometry and Veiling

Figures 2, 9, 16, and 23 show relative brightness in broad photometric bands. Systems are faintest during times of strong polarization, when viewed most nearly along field lines, suggesting optical depth effects in the accretion flow. Figures 3, 10, 17, and 24 show veiling+1, calculated from changes in line depth relative to the mean profile for all 6 nights, averaged over hundreds of photospheric lines. There is no consistent relationship between veiling and polarization, suggesting that stochastic variations in accretion rate, rather than magnetic geometry, control veiling variatons. Unexpectedly, veiling correlates poorly (or is anti-correlated) with photometry.

4. Equivalent Widths, Centroids, and Line Asymmetries

Figures 4, 11, 18, and 25 show selected line profiles for each night with the mean profile for the entire run serving as a reference. Figures 5-7, 12-14, 19-21, and 26-28 show equivalent widths, velocity centroids, and blue/red asymmetries for line profiles. For line pairs in panels (b) and (c), nightly trends are computed by scaling measured parameters for both lines to a common global mean. With the possible exception of AA Tau, He I is redshifted when polarization is strong, implying maximum projected infall velocity occurs at rotational phase when looking along magnetic field lines. Equivalent widths tend to be large when polarization is strongest, suggesting that increased line emission dominates continuum enhancement due to veiling. Asymmetries track centroid behavior well.

References

Johns–Krull, C.M. & Valenti, J.A. 2001, ApJ, 561

Johns–Krull, C.M., Valenti, J.A., Hatzes, A., & Kanaan, A. 1999, ApJ, 510, L41

Vogt, S.S., Tull, R.G., & Kelton, P.W. 1980, ApJ, 236, 308

Figure 1 Magnetic Field BP Tau

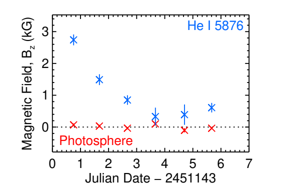

Figure 2 Photometry BP Tau

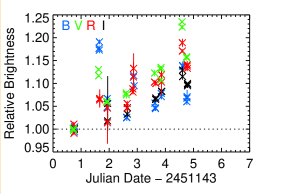

Figure 3 Line Depths BP Tau

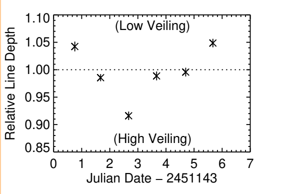

Figure 4a He I 5876 BP Tau

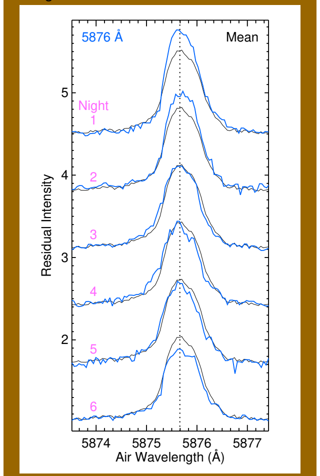

Figure 4b Hα and Hβ BP Tau

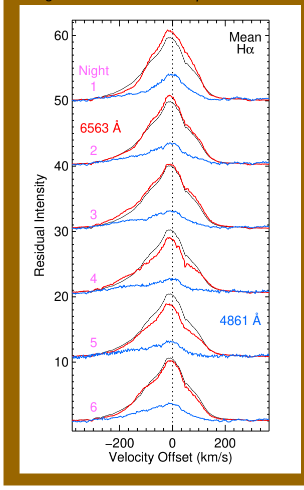

Figure 4c Ca II IRT BP Tau

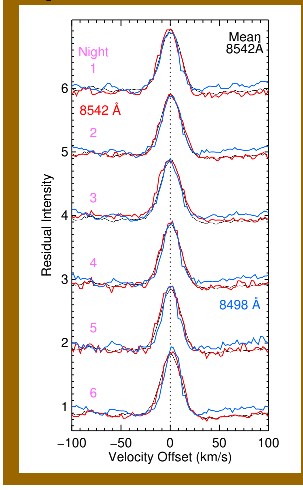

Figure 5a He I 5876 BP Tau

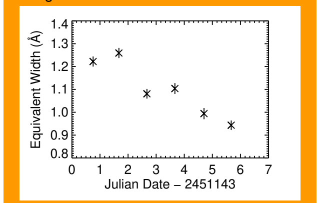

Figure 5b Hα and Hβ BP Tau

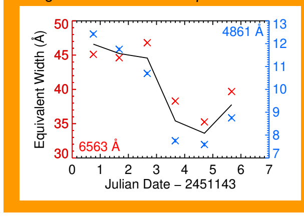

Figure 5c Ca II IRT (core) BP Tau

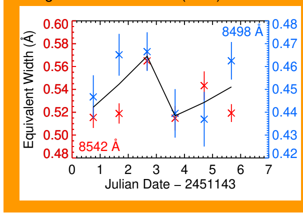

Figure 6a He I 5876 BP Tau

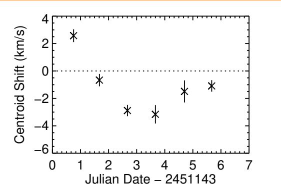

Figure 6b Hα and Hβ BP Tau

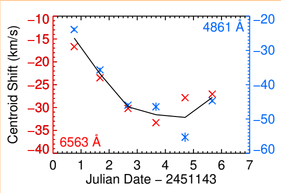

Figure 6c Ca II IRT (core) BP Tau

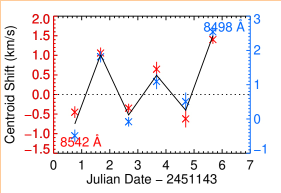

Figure 7a He I 5876 BP Tau

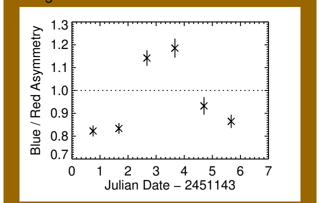

Figure 7b Hα and Hβ BP Tau

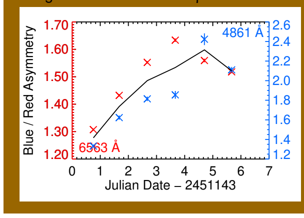

Figure 7c Ca II IRT (core) BP Tau

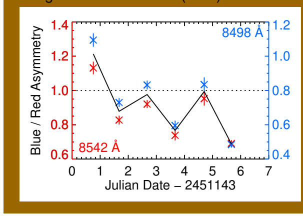

Figure 8 Magnetic Field DF Tau

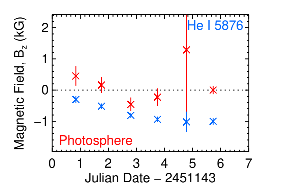

Figure 9 Photometry DF Tau

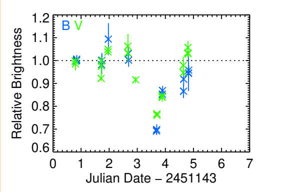

Figure 10 Line Depths DF Tau

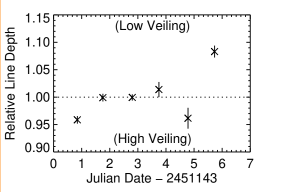

Figure 11a He I 5876 DF Tau

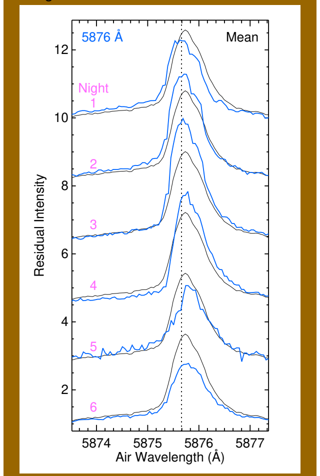

Figure 11b Hα and Hβ DF Tau

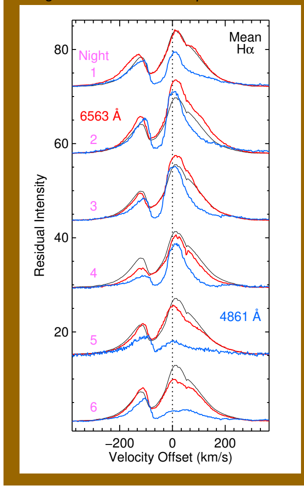

Figure 11c Ca II IRT DF Tau

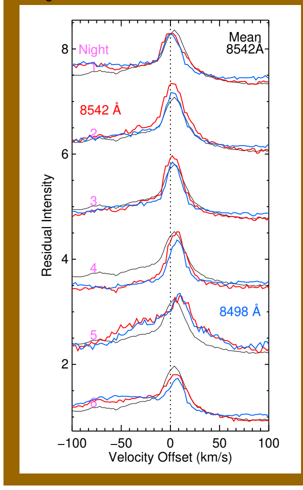

Figure 12a He I 5876 DF Tau

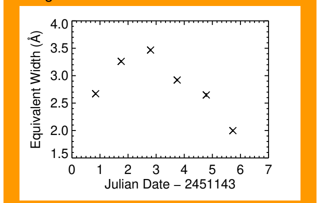

Figure 12b Hα and Hβ DF Tau

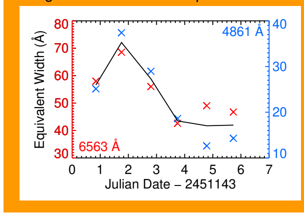

Figure 12c Ca II IRT (core) DF Tau

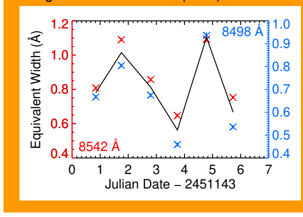

Figure 13a He I 5876 DF Tau

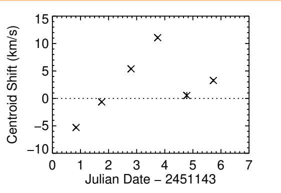

Figure 13b Hα and Hβ DF Tau

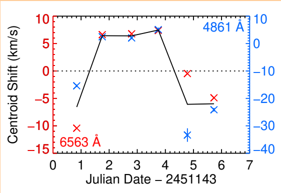

Figure 13c Ca II IRT (core) DF Tau

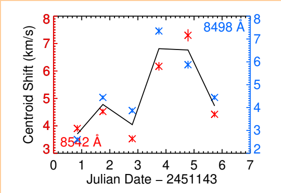

Figure 14a He I 5876 DF Tau

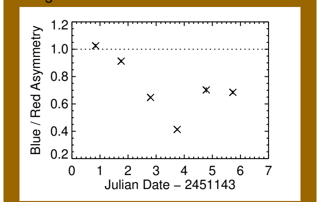

Figure 14b Hα and Hβ DF Tau

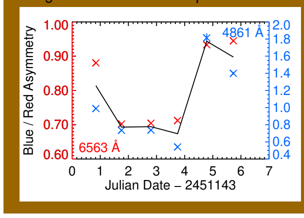

Figure 14c Ca II IRT (core) DF Tau

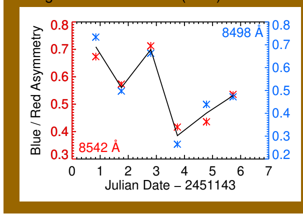

Figure 15 Magnetic Field DK Tau

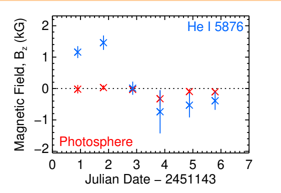

Figure 16 Photometry DK Tau

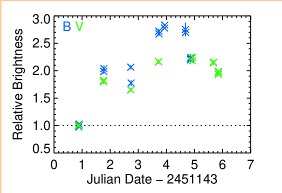

Figure 17 Line Depths DK Tau

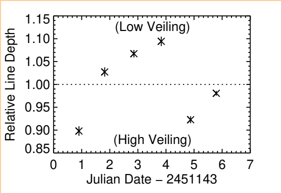

Figure 18a He I 5876 DK Tau

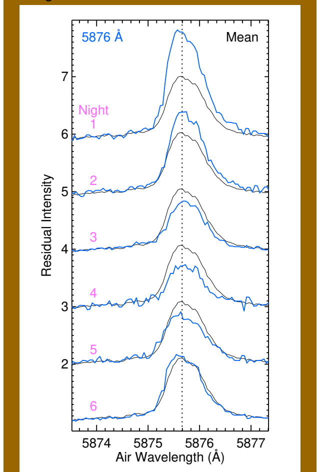

Figure 18b Hα and Hβ DK Tau

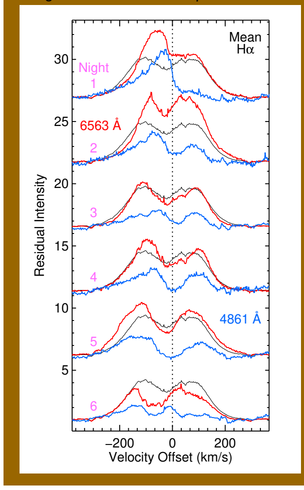

Figure 18c Ca II IRT DK Tau

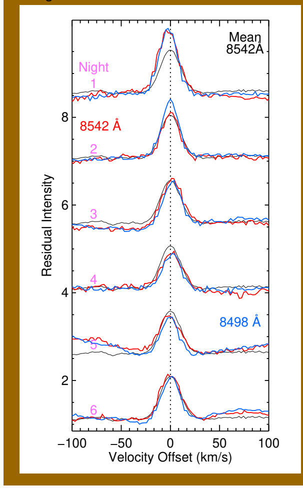

Figure 19a He I 5876 DK Tau

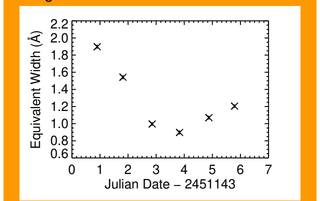

Figure 19b Hα and Hβ DK Tau

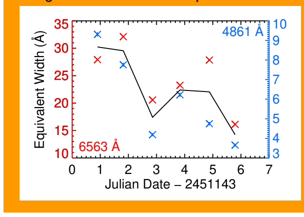

Figure 19c Ca II IRT (core) DK Tau

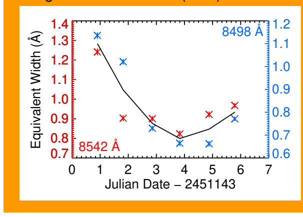

Figure 20a He I 5876 DK Tau

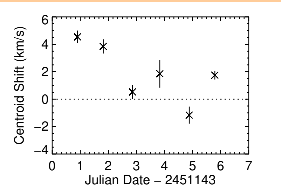

Figure 20b Hα and Hβ DK Tau

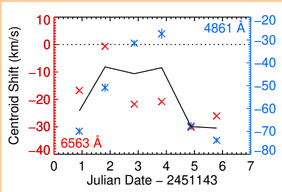

Figure 20c Ca II IRT (core) DK Tau

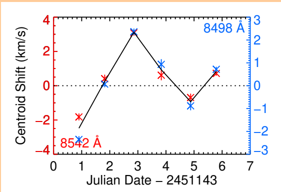

Figure 21a He I 5876 DK Tau

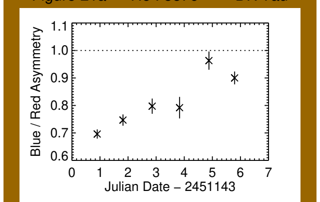

Figure 21b Hα and Hβ DK Tau

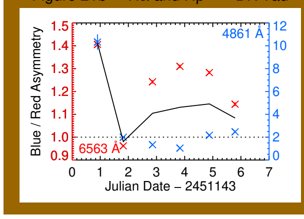

Figure 21c Ca II IRT (core) DK Tau

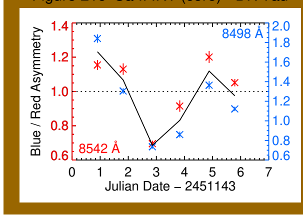

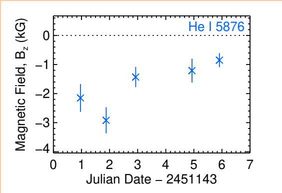

Figure 22 Magnetic Field AA Tau

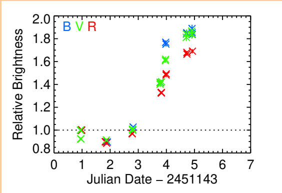

Figure 23 Photometry AA Tau

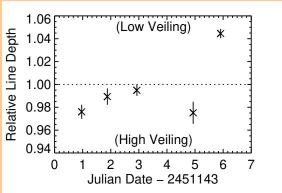

Figure 24 Line Depths AA Tau

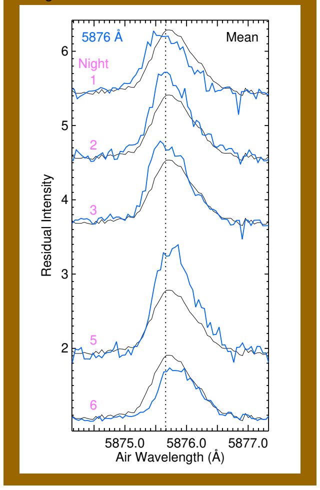

Figure 25a He I 5876 AA Tau

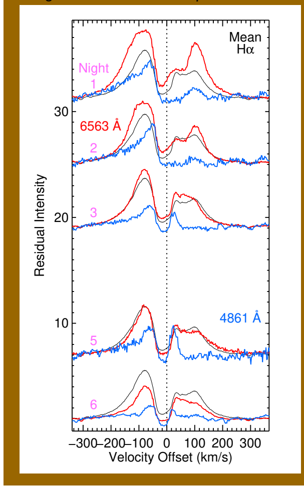

Figure 25b Hα and Hβ AA Tau

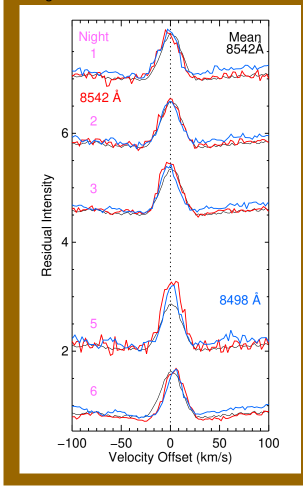

Figure 25c Ca II IRT AA Tau

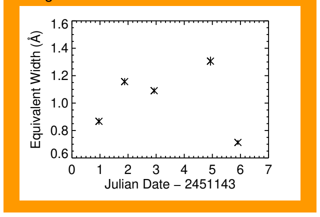

Figure 26a He I 5876 AA Tau

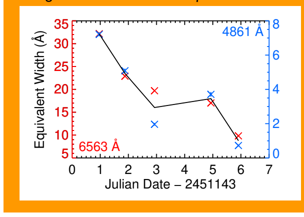

Figure 26b Hα and Hβ AA Tau

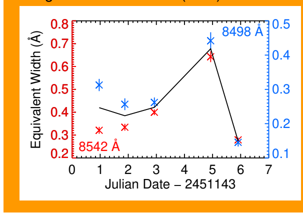

Figure 26c Ca II IRT (core) AA Tau

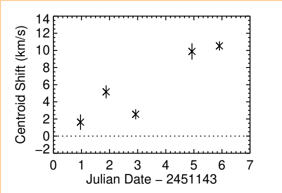

Figure 27a He I 5876 AA Tau

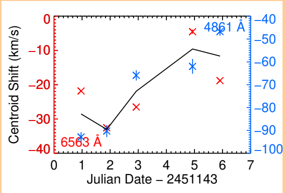

Figure 27b Hα and Hβ AA Tau

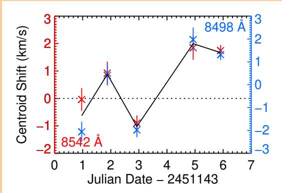

Figure 27c Ca II IRT (core) AA Tau

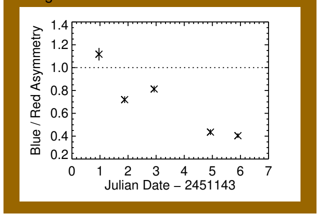

Figure 28a He I 5876 AA Tau

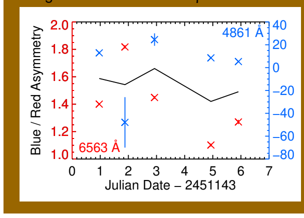

Figure 28b Hα and Hβ AA Tau

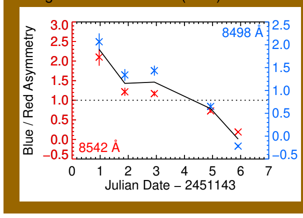

Figure 28c Ca II IRT (core) AA Tau